Indian Journal of Chemistry
Vol. 63, July 2024, pp. 657-663
DOI: 10.56042/ijc.v63i7.5617

1D porous zinc(II) coordination polymer as fluorescent chemosensors for nitrobenzene and Fe^{3+}

Min Deng, Xiao-Dan Fang, Xiao-Yu Li, Wei Guo, Quan-Qing Xu, Ai-Xin Zhu* & Rong-Rong Zhu*

Faculty of Chemistry and Chemical Engineering, Yunnan Normal University, Kunming 650500, P. R. China

E-mail: zaxchem@126.com, chemzrr1993@163.com

Received 16 September 2023; accepted (revised) 25 January 2024

This paper studies the luminescence-sensing properties of 1D porous zinc coordination polymer $[Zn(3\text{-tba})_2]\cdot DMA$ (**1**, 3-Htba = 3-(4*H*-1,2,4-triazol-4-yl)benzoic acid, DMA = *N*,*N*-dimethylacetamide). The systematic luminescence experiments indicate that it can be potentially used as a fast-response fluorescence sensor for the sensitive detection of nitrobenzene and Fe^{3+} ion through drastic fluorescence quenching. Moreover, the quenching mechanisms of **1** towards nitrobenzene and Fe^{3+} have also been investigated.

Keywords: 1D coordination polymer, Luminescence, Sensing, Nitrobenzene, Fe^{3+} ion

Nitrobenzene (NB), the primary component of explosives, is extensively employed in numerous industrial sectors including pesticide production, plastic manufacturing, and aniline synthesis. However, it can cause serious health and environmental problems due to its severe toxicity, carcinogenicity, nondegradability and cumulative effects[1,2]. Iron is a vital element in the composition of the human body, playing a crucial role in various biological and chemical processes at the cellular level. However, the shortage as well as the excess of iron element can cause various serious biological disorders such as anemia, cirrhosis, sepsis, *etc*.[3,4] Therefore, it is very important to develop simple, rapid, effective, low-cost, reliable, and environmentally friendly technologies for sensing hazardous environmental contaminants and metal ions. This is crucial to safeguarding the safety of our health, food, and environment.

During the past two decades, metal-organic frameworks (MOFs) or porous coordination polymers (PCPs), as a new kind of potential multifunctional crystalline materials, have caught significant attention due to their diverse topologies, adjustable microporosity and high surface areas[5,6]. They have been widely used in many areas, including magnetic properties[7], catalysis[8], gas storage or separation[9], drug delivery[10], sensing[11] and so on. Among these applications, luminescent porous coordination polymers (LPCPs) have been regarded as a class of very promising chemosensors[12-14]. This luminescence-based sensing method has the advantages of short response time, easy recyclability, low cost, high sensitivity and efficiency. As a result, various luminescent PCP-based sensors have been developed for fluorescent chemosensors[12-14].

To the best of our knowledge, most luminescent PCPs sensors were constructed by using d^{10} transition metal ions and conjugated organic ligands[14]. The d^{10} metal ions are uneasy to cause fluorescence quenching due to their full electron in orbit structures. Luminescent sensing can be easily realized by the photo-excited electron transfer from π-electron-rich aromatic ligands to the electron-deficient analytes through luminescence quenching. Therefore, the combination of π-electron-rich aromatic ligand and d^{10} metal ions provides a promising method for constructing luminescent PCPs. More recently, azolate-carboxylate bifunctional ligands have attracted considerable attention as useful ligands in the construction of PCPs[15-20]. Additionally, 1D CPs have shown high selectivity and sensitivity as fluorescent sensors for detecting molecules and ions[21-23]. However, until now, there are only a few reported 1D PCPs constructed using d^{10} metal ions and triazolate-carboxylate bifunctional organic ligands for sensing purposes[24].

Previously, we constructed a series of luminescent PCPs by using d^{10} metal ions and bifunctional triazolate-carboxylate ligands 4-(1*H*-1,2,4-triazol-1-yl)benzoic acid (Htba)[25,26], 4-(4*H*-1,2,4-triazol-4-

yl)benzoic acid (4-Htba)[27], 3-(4*H*-1,2,4-triazole-4-yl)benzoic acid (3-Htba)[28]. Very recently, we reported a 1D porous coordination polymer [Zn(3-tba)$_2$]·DMA showing unique vapour-induced reversible switching phenomenon[29]. As an extension of our work on the properties of metal triazolate-carboxylate compounds, the luminescence sensing properties of 1D porous coordination polymer [Zn(3-tba)$_2$]·DMA (**1**) were investigated.

Experimental Section

The compound [Zn(3-tba)$_2$]·DMA (**1**) was prepared according to methods reported in the literature[29]. Other chemicals were obtained from commercial sources and used without further purification. Powder X-ray diffraction (PXRD) measurements were recorded on a Rigaku D/M-2200T automated diffractometer (CuKα, 1.5418 Å). Infrared spectra were obtained from KBr pellets on a Bruker EQUINOX 55 Fourier Transform Infrared spectrometer in the 400-4000 cm^{-1} region. Fluorescence spectrum was recorded with a Hitachi F-4600 fluorescence spectrophotometer at room temperature in the solid state. UV-Vis absorption spectra were carried out on a Hitachi 3310 UV-Vis spectrophotometer. XPS data were obtained using a PHI5000 Versa probe (ULVAC-PHI, INC., Japan) instrument. The HOMO and LUMO orbital enegies were calculated by density functional theory (DFT) at B3LYP/6-31G* accuracy level using the Gaussian 09 package of programs.

Luminescence sensing experiment

In a typical process, the sample of **1** without any activation was ground into a fine powder in an agate mortar, and the powder sample of **1** (3 mg) was dispersed in 5 mL DMF solvent by ultrasonication for 30 min to obtain a well-distributed suspension (**1**, DMF). The suspension of **1** (3 mL) was injected into a 1 cm × 1 cm quartz cell for fluorescence measurements. For the sensing of nitrobenzene, a 300 μL amount of each analyte (10 mM) was added to the **1**-DMF suspension. For the sensing of Fe^{3+}, a 100 μL amount of each analyte (10 mM) was added to the **1**-DMF suspension. Detailed detections for all titrates were carried out by gradually adding nitrobenzene (1 × 10^{-2} M) and Fe^{3+} (6 × 10^{-3} M) DMF solutions in an incremental fashion. Each independent sensing experiment was repeated at least three times to get a concordant value. In the time-dependent tests, a 300 μL DMF solution of nitrobenzene (10 mM) and a 100 μL DMF solution of Fe^{3+} (10 mM) were added to the **1**-DMF suspension, and the luminescence intensity was measured at a certain time interval. For the recyclability experiments, the titration maximum dose was added to the **1**-DMF suspension, and the suspension was shaken for ten minutes. Compound **1** can be regenerated by filtering the solution after use and washing several times with DMF to remove nitrobenzene molecules and Fe^{3+}. All luminescence measurements were done at 298 K. The emission spectrum of the **1**-DMF suspension in the range of 317-600 nm was recorded with the maximum emission wavelength at 367 nm (λ_{ex} = 317 nm), the slit widths of excitation and emission were fixed at 2.5 nm. The quenching efficiency was calculated as $[(I_0 - I) / I_0] \times 100\%$, where I_0 and I are the luminescent intensity of the **1**-DMF suspension before and after the analyte incorporation.

Results and Discussion

Structure Description

In our previous study, we successfully determined the single-crystal structure of [Zn(3-tba)$_2$]·DMA using single-crystal X-ray diffraction[29]. As shown in Fig. 1, it exhibits a 1D chain structure composed of [Zn$_2$(3-tba)$_2$] rings, which are interconnected by adjacent Zn(II) ions and pairs of V-shaped, 3-tba linkers. The crystal packing results in 1D rhombic channels with effective pore diameter of 4.9 × 7.3 Å^2, and it contains the calculated guest-accessible volume of 27.4%, which is occupied by DMA guest molecules.

Photoluminescence Properties

The solid-state luminescent properties of free ligand 3-Htba and compound **1** were investigated at room temperature, as displayed in Fig. 2, The luminescent spectra of the free ligand 3-Htba has the main emission peak at 432 nm under 322 nm excitation, which may be attributed to the π* - n or π*

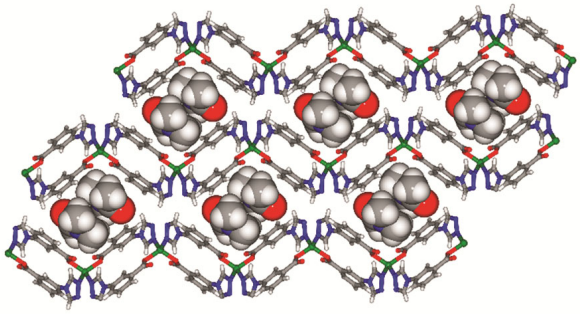

Fig. 1 — The packing diagrams of compound **1** viewed along the *a*-axis (DMA molecules are showing with the space-filling mode)

- π electron transition[25-28]. Compound **1** displays purple emissions with the maximum emission peak at 419 nm upon the excitation at 313 nm. Due to its d^{10} electronic configuration of the Zn(II) ions, which are difficult to oxidize or to reduce, the emissions of **1** are neither metal-to-ligand charge transfer (MLCT) nor ligand-to-metal charge transfer (LMCT). Thus, the emissions can be attributed to intra-ligand electron transitions or ligand-to-ligand charge transfer (LLCT) in the 3-Htba ligands[30,31]. Compared with the free ligand 3-Htba, the maximum emission of compound **1** is obvious blue-shift of approximately 13 nm, which is mainly due to the coordination of the ligand to the metal[32]. The fluorescence of the free 3-Htba ligand and **1** dispersed in DMF solution were also recorded. As shown in Fig. S2, The luminescent spectra of the free ligand 3-Htba has the main emission peak at 400 nm under the excitation of 332 nm, Compound **1** displays the maximum emission peak at 368 nm upon the excitation at 317 nm.

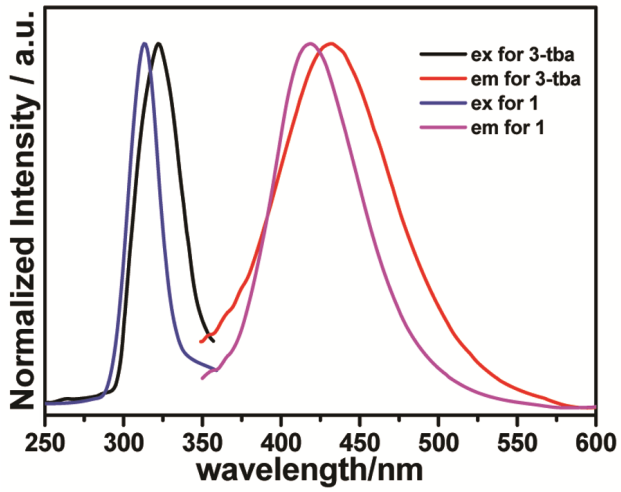

Fig. 2 — Luminescence spectra of **1** and the free ligand 3-Htba in the solid state at room temperature

Sensitization of organic solvent molecules

To probe the sensing capabilities of **1**, DMF was chosen as the dispersed solvent in the experiments. Furthermore, the PXRD analyses revealed that **1** can retained its framework structure after being immersed in DMF solvent for two days (Fig. S1). A 300 μL DMF solution (10 mM) containing different organic solvent molecules such as methanol, ethanol, acetonitrile, acetone, dichloromethane (CH_2Cl_2), trichloromethane ($CHCl_3$), dimethyl sulfoxide (DMSO), benzene, toluene, chlorobenzene and nitrobenzene (NB) was added to 3 mL suspension of **1** in DMF. The results depicted in Fig. 3a and Fig. 3b demonstrate that nitrobenzene

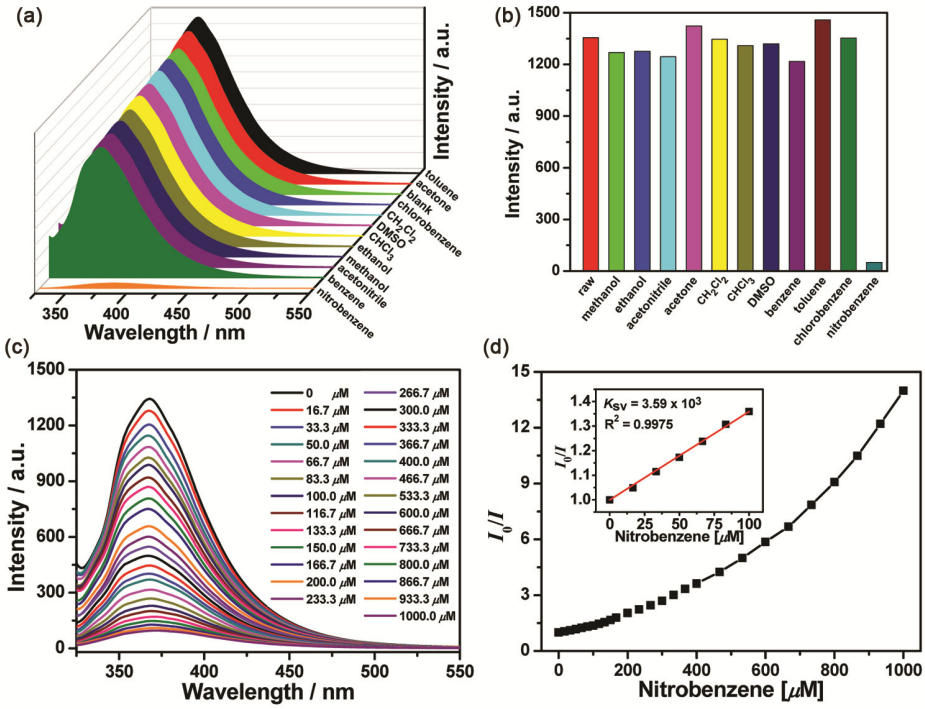

Fig. 3 — (a) The emission spectra of **1**-DMF suspensions in the presence of 300 μL different analytes (λ_{ex} = 317 nm); (b) Comparison of the luminescence intensities of **1**-DMF suspensions in the presence of 300 μL different analytes; (c) Luminescence spectra of **1**-DMF suspensions with different concentrations of NB. (d) The Stern-Volmer plots for the **1-DMF** suspensions with NB. Inset: [Nitrobenzene] ≤ 100 μM.

significantly quenches the luminescent intensity, while the others solvents exhibit no significant effect. This suggests that **1** has the potential to be used as a luminescence sensor for detecting NB molecules.

To further investigate the luminescent sensing ability of NB, we conducted fluorescence quenching titrations. As NB is incrementally introduced to the **1**-DMF suspension, the luminescence intensity exhibits a gradual decrease in correlation with the concentration of NB (Fig. 3c). At a 1000.0 μM concentration of NB, the luminescence intensity is nearly completely quenched with a high quenching efficiency of 93.0%.

The luminescence quenching effect of **1** can be further quantitatively evaluated by the Stern-Volmer (SV) equation: $I_0/I = K_{sv}[A] + 1$ (I_0 and I are the luminescent intensity of the **1**-DMF suspension before and after incorporation of the analytes, respectively; [A] is the molar concentration of the analytes, and K_{sv} is the quenching constant (M^{-1})). As shown in Fig. 3d, the Stern-Volmer plot of NB exhibits a linear increase at low concentrations (≤ 100 μM), followed by a deviation from linearity. At higher concentrations, the plot bends upwards, indicating a potential influence of self-absorption or an energy-transfer process[33]. The K_{sv} value of **1** towards NB is 3.59×10^3 M^{-1}, which is comparable to those of some previously reported 1D d^{10} PCPs (Table S1)[34,35].

In order to study time-dependent luminescence quenching caused by NB, a 300 μL DMF solution of NB was introduced into the **1**-DMF suspension, the luminescence intensity of **1** was rapidly quenched in only 16 seconds (Fig. 4), which suggests that **1** can serve as a rapid response and highly sensitive sensor for NB. Furthermore, the recyclability of **1** for detecting nitrobenzene was also assessed. As shown in Fig. 5, it can proceed with five cycles without any obvious intensity loss, which suggests that **1** displays a good recyclability for detection applications.

The underlying mechanism of the quenching effect of **1** by nitrobenzene has been explored in detail. The PXRD patterns indicate that the crystal structure of **1** is still retained after being immersed in various analytes for one day (Fig. S3). The luminescence quenching of **1** is unlikely attributed to the adsorption by the nitrobenzene molecule because nitrobenzene does not exhibit any UV adsorption bands above 320 nm (Fig. S4). The Stern-Volmer curve was nearly linear at low concentrations and deviated from linearity at high concentrations (Fig. 3d), which is normally owing to the presence of two distinct quenching mechanisms: electron transfer or energy transfer[36]. In order to understand the electron transfer process in luminescence quenching, density functional theory at the B3LYP/6-31G* level was applied to calculate the molecular orbital energy for the ligand 3-Htba and the selected analytes. As shown in Fig. 6, the LUMO energy of the electron-rich ligand 3-Htba was calculated to be -1.96 eV, which is lower than those of benzene (0.10 eV), toluene (0.14 eV) and chlorobenzene (-0.34 eV), but higher than that of NB (-2.43 eV). These LUMO energy values suggest that the photo-induced electron transfer can take place from electron-rich **1** to electron-deficient NB, leading to the quenching of the photoluminescence in **1**[37,38]. Moreover, the UV absorption spectra show that the absorption bands of nitrobenzene partly overlap with the excitation bands of **1** between 275 nm and 360 nm, whereas other selected molecules such as benzene, toluene and chlorobenzene show no adsorption bands in this range

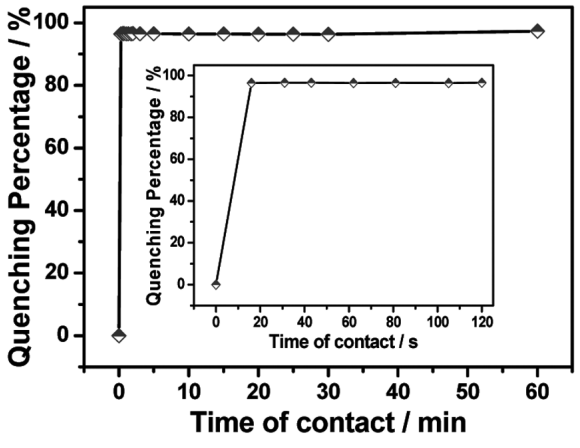

Fig. 4 — Time-dependent luminescence quenching of **1** by nitrobenzene. Inset: [Time] ≤ 2 min.

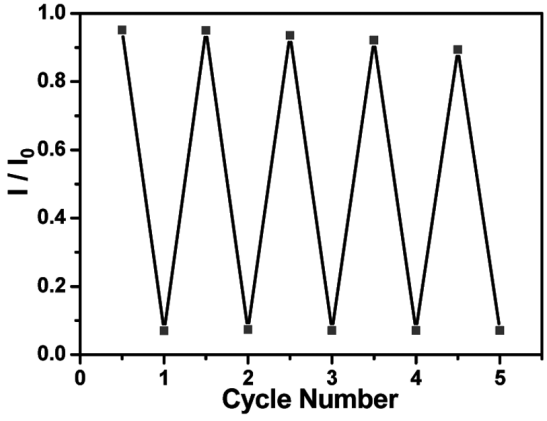

Fig. 5 — Recyclability tests of **1** in the presence of nitrobenzene

(Fig. S5), which further indicates that resonance energy transfer can take place between **1** and nitrobenzene[39]. All these results show that the coexistence of electron transfer and resonance energy transfer is the reason for the photoluminescence quenching of NB.

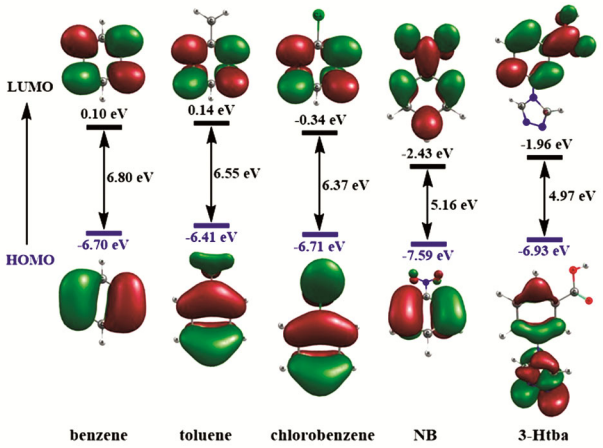

Fig. 6 — HOMO and LUMO energy levels of benzene, toluene, chlorobenzene, NB and the ligand 3-Htba

Detection of metal cation

In order to investigate the sensing ability of **1** for metal ions, a 100 μL DMF solution (10 mM) containing different metal ions such as $M(NO_3)_n$ (M = Na^+, Mg^{2+}, Ca^{2+}, Pb^{2+}, Zn^{2+}, Cd^{2+}, Ag^+, Mn^{2+}, Co^{2+}, Ni^{2+}, Cu^{2+}, Al^{3+}, Cr^{3+}, Fe^{3+}, respectively) was added to a suspension of **1** in DMF (3 mL). As shown in Fig. 7a and Fig. 7b, Fe^{3+} causes a significant quenching effect on luminescence of **1**, Cu^{2+} ions cause a moderate decline in luminescence intensity, and other metal ions has no significant effect on luminescence intensity. The remarkable changes of luminescence intensity caused by Fe^{3+} indicate that **1** can be considered as a promising luminescent probe of Fe^{3+} through fluorescent quenching.

Luminescence titration experiments were performed to better understand the variation of luminescence intensity with the concentration of Fe^{3+}. As the concentration of Fe^{3+} gradiently increased, the luminescence intensity of the **1**-DMF suspension was gradually quenched (Fig. 7c). The quenching efficiency was approximately 94.0% for **1** at a 320 μM concentration of Fe^{3+}. The luminescence quenching ability can be analyzed by the Stern-Volmer (SV)

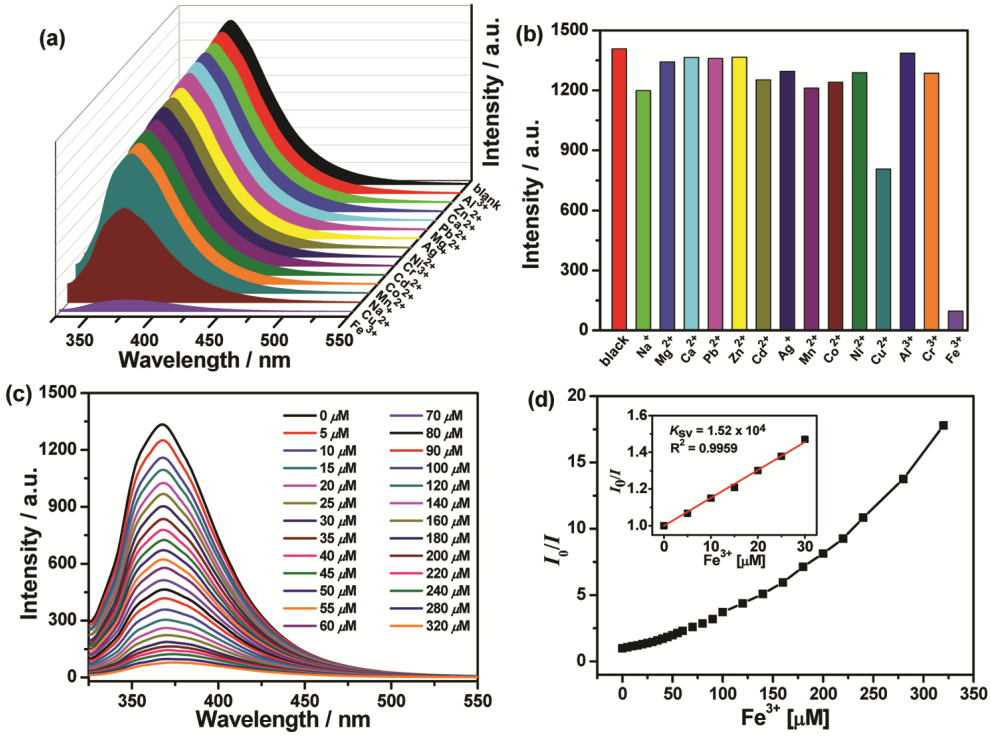

Fig. 7 — (a) The emission spectra of the luminescence intensities of **1** dispersed in DMF upon addition of 100 μL of metal ions (10 mM) (λ_{ex} = 317 nm); (b) The comparison of the luminescence intensities of **1** dispersed in DMF upon addition of 100 μL of metal ions (10 mM); (c) Luminescent quenching of **1** dispersed in DMF with gradual addition of Fe^{3+} (λ_{ex} = 317 nm); (d) Plots of relative intensity *vs.* Fe^{3+} concentration for **1**. Inset: $[Fe^{3+}] \leq 30$ μM.

equation: $I_0 / I = K_{sv}[A] + 1$. As shown in Fig. 7d, the Stern-Volmer plot of Fe^{3+} shows a linear increase at low concentrations (≤ 30 μM) and subsequently deviated from linearity, bending upwards at higher concentrations. The calculated K_{sv} value is 1.52×10^4 M^{-1}, which are much better than those of some previously reported Zn(II)- or Cd(II)-based PCPs (Table S2)[21,40-43], In order to study the quenching speed of Fe^{3+}, time-dependent emission intensity was also investigated. As shown in Fig. S6, the luminescence intensity was completely quenched within 16 seconds, which suggests that compound **1** can be used as a rapidly sensitive sensor for Fe^{3+}. The recyclability experiments for sensing Fe^{3+} indicate that **1** possesses a good recyclability because the luminescence intensity is basically maintained after five quenching-recovery cycles (Fig. S7).

In order to explore the quenching mechanism caused by Fe^{3+} ion, the following discussions were proposed: firstly, the PXRD analyses confirm that **1** still maintains its original framework after being immersed in various metal ions solutions for one day (Fig. S8), which suggests that the quenching mechanism does not involve the collapse of the framework structure. Secondly, the UV-Vis absorption spectra of the metal ions indicate an obvious overlap between the absorption bands of Fe^{3+} and the excitation bands of **1** dispersed in DMF within the range of 285 nm to 360 nm (Fig. S9). This observation suggests the presence of notable competitive absorption of the exciting light between Fe^{3+} ions and **1**[44]. Thus, the UV-Vis absorption of Fe^{3+} ions can hinder the absorption of **1**, resulting in the quenching of luminescence. Thirdly, the color of **1** changed after immersion in $Fe(NO_3)_3$ (10^{-2} M) solutions of DMF, followed by washing with DMF several times (Fig. S10). X-ray photoelectron spectroscopy (XPS) reveals that the N 1s peaks of **1** remain relatively unchanged after the introduction of Fe^{3+}, but the O 1s peaks of **1** at 530.9 eV shift to 531.3 eV (Fig. S11-S13). These results reveal that Fe^{3+} ions weakly bond with oxygen atoms from triazolate-carboxylate ligand. Therefore, this weak bonding may also change the electron energy level of ligand and hinder the absorption of **1** upon excitation, leading to luminescence quenching.

Conclusions

In summary, we study the luminescence sensing properties of 1D porous coordination polymer $[Zn(3\text{-tba})_2]\cdot DMA$. The fluorescence experiments demonstrate its rapid response (<16 seconds), high sensitivity and excellent recyclability in detecting nitrobenzene and Fe^{3+} through drastic luminescence quenching effects, suggesting its potential as a candidate for sensing these substances. PL fluorescence titrations, UV absorption spectra and density functional theory calculations indicate that the photoluminescence quenching by nitrobenzene is ascribed to electron transfer and resonance energy transfer. PXRD, XPS, and UV-Vis absorption spectra confirm that the quenching caused by Fe^{3+} is a result of the competitive absorption of the exciting light, along with weak bonding interaction between Fe^{3+} ions and **1**.

Supplementary Information

Supplementary information is available in the website http://nopr.niscpr.res.in/handle/123456789/58776.

Acknowledgements

This work is financially supported by the National Natural Science Foundation of China (21661035 and 21261028). We also thank Wei-Hua Mu from Yunnan Normal University for the molecular orbital energy calculations.

References

1 Yang L, Lian C, Li X, Han Y, Yang L, Cai T & Shao C, *ACS Appl Mat Interfaces*, 9 (2017) 17208.
2 Du Y, Yang H, Liu R, Shao C & Yang L, *Dalton Trans*, 49 (2020) 13003.
3 Sahoo S K, Sharma D, Bera R K, Crisponic G & Callan J F, *Chem Soc Rev*, 41 (2012) 7195.
4 Zhou W, Saran R & Liu J, *Chem Rev*, 117 (2017) 8272.
5 Lu W, Wei Z, Gu Z Y, Liu T F, Park J, Park J, Tian J, Zhang M, Zhang Q, Gentle T, Bosch M & Zhou H C, *Chem Soc Rev*, 43 (2014) 5561.
6 Kitagawa S, Kitaura R & Noro S, *Angew Chem Int Ed*, 43 (2004) 2334.
7 Coronado E & Espallargas G M, *Chem Soc Rev*, 42 (2013) 1525.
8 Yoon M, Srirambalaji R & Kim K, *Chem Rev*, 112 (2012) 1196.
9 Li J R, Sculley J & Zhou H C, *Chem Rev*, 112 (2012) 869.
10 Lawson H D, Walton S P & Chan C, *ACS Appl Mat Inter*, 13 (2021) 7004.
11 Lustig W P, Mukherjee S, Rudd N D, Desai A V, Li J & Ghosh S K, *Chem Soc Rev*, 46 (2017) 3242.
12 Kreno L E, Leong K, Farha O K, Allendorf M, Duyne R P V, & Hupp J T, *Chem Rev*, 112 (2012) 1105.
13 Zhang Y, Yuan S, Day G, Wang X, Yang X & Zhou H C, *Coord Chem Rev*, 354 (2018) 28.
14 Hu Z, Deibert B J & Li J, *Chem Soc Rev*, 43 (2014) 5815.
15 Wang T, Mei W, Li P, Peng Y L, Chen Y, Ma J G, Cheng P, Fang M, Yu K & Zhang Z, *J Mater Chem A*, 10 (2022) 22175.
16 Yang S Q, Zhou L, He Y, Krishna R, Zhang Q, An Y F, Xing B, Zhang Y H & Hu T L, *ACS Appl Mater Interfaces*, 14 (2022) 33429.

17 Cheng H, Wang Q, Meng L, Sheng P, Zhang Z, Ding M, Gao Y & Bai J, *ACS Appl Mater Interfaces*, 13 (2021) 40713.
18 Menzel S, Heinen T, Boldog I, Beglau T H Y, Xing S, Spieß A, Woschko D & Janiak C, *CrystEngComm*, 24 (2022) 3675.
19 Albalad J, Peralta R A, Huxley M T, Tsoukatos S, Shi Z, Zhang Y B, Evans J D, Sumby C J & Doonan C J, *Chem Sci*, 12 (2021) 14893.
20 Menzel S, Millan S, Höfert S P, Nuhnen A, Gökpinar S, Schmitz A & Janiak C, *Dalton Trans*, 49 (2020) 12854.
21 Lin Y, Zhang X, Chen W, Shi W & Cheng P, *Inorg Chem*, 56 (2017) 11768.
22 Li B, Yan Q Q & Yong G P, *J Mater Chem C*, 8 (2020) 11786.
23 Peng Q, Liu X & Zhou J, *J Mate Chem C*, 10 (2022) 6365.
24 Zhang S S, Yan Y T, Zhang W Y, Fan Y K, Zhang Y, Zhong K & Wang Y Y, *Inorg Chim Acta*, 495 (2019) 118971.
25 Zhu A X, Qiu Z Z, Yang L B, Fang X D, Chen S J, Xu Q Q & Li Q X, *CrystEngComm*, 17 (2015) 4787.
26 Fang X D, Yao J, Fan R, Bai X F, Liu Y E, Hou C F, Xu Q Q, Zhu A X & Huang B, *J Solid State Chem*, 294 (2021) 121854.
27 Yang L B, Wang H C, Fang X D, Chen S J, Xu Q Q, Zhu A X & Yang Z, *CrystEngComm*, 18 (2016) 130.
28 Yang L B, Wang H C, Dou A N, Rong M Z, Zhu A X & Yang Z, *Inorg Chim Acta*, 446 (2016) 103.
29 Deng M, Mukherjee S, Liang Y J, Fang X D, Zhu A X & Zaworotko M J, *Chem Commun*, 58 (2022) 8218.
30 An F, Zhang C, Duan L, Liu X, Wang Z, Jin X & Song W, *New J Chem*, 43 (2019) 4800.
31 Deng L, Zhang Y, Zhang D, Jiao S, Xu J, Liu K & Wang L, *CrystEngComm*, 21 (2019) 6056.
32 Jin S S, Han X, Yang J, Zhang H M, Liu X L & Ma J F, *J Lumin*, 188 (2017) 346.
33 Nagarkar S S, Desai A V & Ghosh S K, *Chem Commun*, 50 (2014) 8915.
34 Tsai M J, Li C Y & Wu J Y, *Cryst Eng Comm*, 20 (2018) 6762.
35 Zhao Q & Si C D, *Cryst Res Technol*, 54 (2019) 1800155.
36 Gole B, Bar A K & Mukherjee P S, *Chem Eur J*, 20 (2014) 2276.
37 Song J H, Kim Y, Lim K S, Kang D W, Lee W R & Hong C S, *Inorg Chem*, 56 (2017) 305.
38 Buragohain A, Yousufuddin M, Sarma M & Biswas S, *Cryst Growth Des*, 16 (2016) 842.
39 Xu T Y, Li J M, Han Y H, Wang A R, He K & Shi Z F, *New J Chem*, 44 (2020) 4011.
40 Fan Y P, Kang Y F, Liang X Q, Li Q Q, Zhang W Q, Liu P & Wang Y Y, *J Inorg Organomet Poly*, 27 (2017) 1376.
41 Wang D, Wang M, Chen K, You Y, Zhang J, Zhou X & Huang W, *Appl Organomet Chem*, 34 (2020) e5692.
42 He Y C, Wu S, Zhang J, Qin W H, Liu J, Zhao F H, Liu L & Jing Z, *CrystEngComm*, 24 (2022) 6715.
43 Fan X F, Li D Y, Deng X C, Fu L & Cui G H, *Polyhedron*, 241 (2023) 116456.
44 Wang J, Wu X R, Liu J Q, Li B H, Singh A, Kumar A & Batten S R, *CrystEngComm*, 19 (2017) 3519.